Applied Surface Science 258 (2012) 8177–8184

Contents lists available at SciVerse ScienceDirect

Applied Surface Science

journal homepage: www.elsevier.com/locate/apsusc

Insight into CH_4 dissociation on NiCu catalyst: A first-principles study

Hongyan Liu[a,b], Riguang Zhang[a], Ruixia Yan[a], Jingrui Li[a], Baojun Wang[a,*], Kechang Xie[a]

[a] Key Laboratory of Coal Science and Technology of Ministry of Education and Shanxi Province, Taiyuan University of Technology, Taiyuan 030024, China
[b] College of Chemistry and Chemical Engineering, Shanxi Datong University, Datong 037009, Shanxi Province, China

ARTICLE INFO

Article history:
Received 20 March 2012
Received in revised form 3 May 2012
Accepted 3 May 2012
Available online 11 May 2012

Keywords:
NiCu alloy
CH_4 dissociation
Reaction barrier
Density functional theory

ABSTRACT

A density-functional theory method has been conducted to investigate the dissociation of CH_4 on NiCu (1 1 1) surface. Two models: uniform surface slab model (Model A) and Cu-rich surface slab model (Model B) have been constructed to represent the NiCu (1 1 1) surface, in which the ratio of Ni/Cu is unit. The obtained results on the two models have been compared with those obtained on pure Ni (1 1 1) and Cu (1 1 1). It is found that the adsorption of CH_x(x = 1–3) on Model B are weaker than on Model A. The rate-determining steps of CH_4 dissociation on Model A and B both are the dissociation of CH, and the corresponding activation barriers are 1.37 and 1.63 eV, respectively. Obviously, it is approximately equal on Model A to that on pure Ni (1 1 1) [H. Liu, R. Zhang, R. Yan, B. Wang, K. Xie, Applied Surface Science 257 (2011) 8955], while it is lower by 0.58 eV on Model B compared to that on pure Cu (1 1 1). Therefore, the Cu-rich surface has better carbon-resistance ability than the uniform one. Those results well explain the experimental facts that NiCu/SiO_2 has excellent catalytic performance and long-term stability [H.-W. Chen, C.-Y. Wang, C.-H. Yu, L.-T. Tseng, P.-H. Liao, Catalysis Today 97 (2004) 173], however, there is serious carbon deposition on NiCu/MgO–Al_2O_3 in CO_2 reforming of methane [J. Zhang, H. Wang, A. K. Dalai, Journal of Catalysis 249 (2007) 300].

1. Introduction

The growing interesting in CO_2 reforming of CH_4 to produce synthesis gas has stimulated extensive work on the research in Ni-based catalysts [1–5]. The reforming reaction not only reduces greenhouse gas emission, but also produces synthesis gas with the ratio of CO and H_2 to unit which is more preferable feed for some liquid fuel synthesis processes. In addition, Ni has good initial activity for the reforming reaction and its cost is low. However, the troublesome carbon deposition restricts the industrialization process.

Recently, Ni-based bimetallic catalysts have been reported that they can affect the catalytic behavior and carbon deposition [6–9]. Chen et al. [10] reported that NiCu/SiO_2 has excellent catalytic performance and long-term stability for CO_2 reforming of methane at 800 °C. However, Wang and co-workers [11] observed serious carbon deposition on NiCu/MgO–Al_2O_3. Why is there so big difference in the experimental results of NiCu catalysts? Many factors, such as the surface structure of active component, the electronic structure of Ni-Cu and metal-support interaction etc., may vary with the addition of copper into supported Ni catalyst system [10]. Moreover, the structures of the Ni-Cu surface have been shown to be sensitive to temperature, suggesting that the formation of carbon on the surface depends strongly on the morphology of the copper and nickel on the surface [12,13]. Meanwhile, Cu is likely to form homogeneous structures with Ni [14], or segregate on Ni surface [15,16].

Carbon mainly results from CH_4 dissociation from thermodynamic viewpoint [17]. In addition, isotopic studies and forward rate measurements confirmed the mechanistic equivalence among CH_4-reforming and decomposition of CH_4 on Ni-based catalysts [18]. Therefore, the chemistry of the successive dehydrogenation reactions of methane is believed to be the key to understanding the formation of carbon.

In recent years, computational methods have become a powerful research tool for understanding the chemical reactions in microscopic view. For example, methods based on quantum-chemical theory provide information at atomic/molecular level [19–21]. In this contribution, we present a systematic study on the successive dehydrogenation of CH_4 on two kinds of NiCu (1 1 1) surfaces using density functional theory (DFT) method. The adsorption geometries and energetics of CH_4 sequence dehydrogenation products on NiCu (1 1 1) have been investigated. Based on the optimized adsorption geometries, the decomposition of CH_4 was first analyzed. Then, the results are compared with those obtained on pure Ni (1 1 1) and Cu (1 1 1) surfaces. It is noted that only the effects of active component on the reaction are considered, while other factors are beyond in this work.

* Corresponding author. Tel.: +86 351 6018239; fax: +86 351 6041237.
E-mail address: Wangbaojun@tyut.edu.cn (B. Wang).

0169-4332/$ – see front matter © 2012 Elsevier B.V. All rights reserved.
http://dx.doi.org/10.1016/j.apsusc.2012.05.017

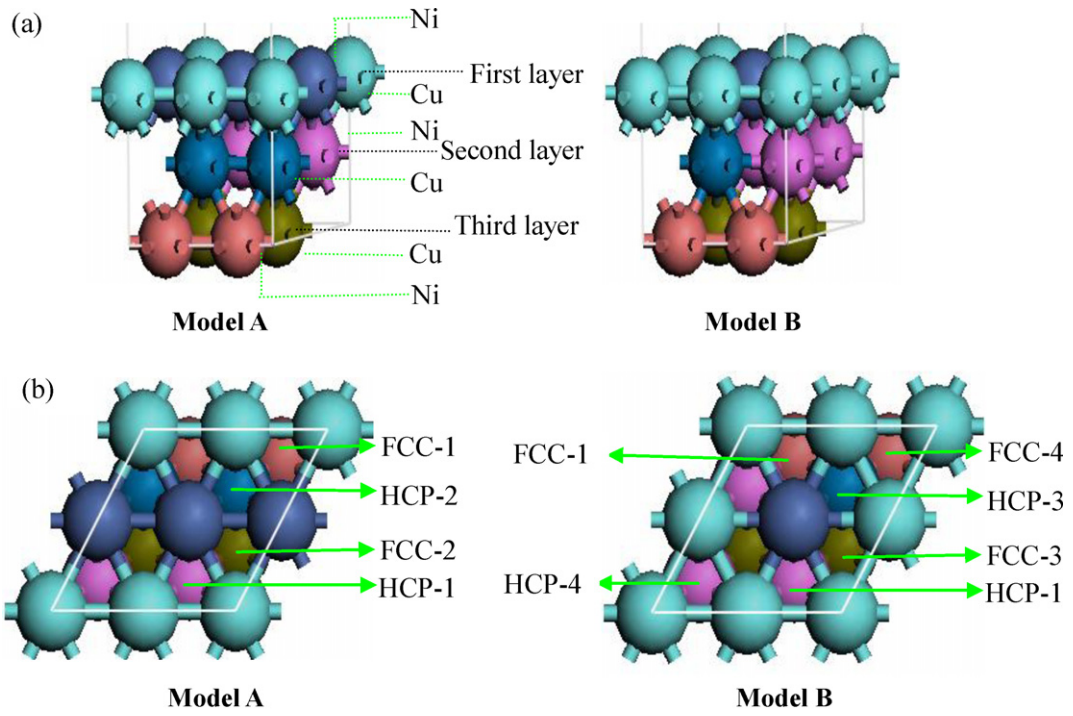

Fig. 1. The surface and the adsorption sites on Model A and Model B of NiCu (1 1 1) (a) side view, (b) top view.

2. Computational details

2.1. Models

It is known that copper and nickel, which have similar lattice constants, can easily form a stable face-centered-cubic (FCC) NiCu alloy system according to the Ni-Cu phase diagram [22], and the alloy system is compositionally homogeneous. Thus, the bulk, including of the 1:1 Ni-Cu binary system, was modeled by replacing half the Ni atoms in a FCC Ni_4 conventional cell with Cu atoms. The lattice constants a and c in the current calculations are 3.559 and 3.616 Å, respectively, which has only slightly modified compared to the lattice parameters of Ni bulk (3.541 Å).

The surfaces were obtained by cutting alloy of NiCu along [1 1 1] direction, the thickness of each surface slab was chosen to be at least as thick as a three-layer slab, which is proved to be reasonable to investigate the adsorption and reaction mechanism in previous literatures [23–25]. The vacuum region between adjacent slabs was in excess of 10 Å. In order to increase the calculation efficiency, the bottom layer of slab was fixed at its equilibrium bulk phase position, while the top two layers and the adsorbates were allowed to relax freely. A (2×2) supercell was used in the calculation in order to reduce interaction between adsorbates on the surface. Herein, we can obtain the uniform slab model, denoted Model A (shown in Fig. 1). However, the composition varies nonmonotonically near the surface, that is, the surface layer is strongly enriched in Cu while the near-surface layers are enriched in Ni [16]. Therefore, the other model was built, i.e., we exchange a Ni atom on the surface layer with a Cu atom on the subsurface layer to obtain Model B (shown in Fig. 1), which expresses that Cu segregates on the surface layer and Ni accumulates on the subsurface layer.

2.2. Methods

Density functional theory (DFT) calculations were performed using the Cambridge Sequential Total Energy Package (CASTEP) [26,27]. All calculations were conducted with the generalized gradient approximation (GGA) with the Perdew–Burke–Ernzerhof (PBE) exchange correlation functional [28]. Ionic cores were described by ultrasoft pseudopotential [29] and the Kohn–Sham one-electron states were expanded in a plane wave basis set up to a cutoff of 340 eV in order to obtain accurate energetics for all systems. A Fermi smearing of 0.1 eV was utilized and the corrected energy extrapolated to 0 K. Brillouin zone integration was approximated by a sum over special k-points chosen using the Monkhorst–Pack method [30], and they were set up to $5 \times 5 \times 1$. Geometries were optimized until the energy had converged to 2.0×10^{-5} eV/atom and the force converged to 0.05 eV/Å and the max displacement converged to 2×10^{-3} Å. Spin polarization was considered in all calculations.

The chemisorption energy, E_{ads}, was calculated as follows:

$$E_{ads} = E_{adsorbates/slab} - (E_{adorbates} + E_{slab})$$

where $E_{adsorbates/slab}$ is the total energies of adsorbates on slab model, $E_{adsorbates}$ is the total energy of isolated adsorbates which was calculated by putting isolated adsorbates in a cubic box of 10 Å × 10 Å × 10 Å, E_{slab} is the total energy of slab.

The reaction energy was calculated by the definition given as follows:

$$\Delta E = \left(E_{A/slab} + E_{B/slab}\right) - \left(E_{AB/slab} + E_{slab}\right)$$

where $E_{A/slab}$, $E_{B/slab}$ and $E_{AB/slab}$ are the total energies of adsorbates A, B and AB adsorption on slab surface, respectively, E_{slab} is the total energy of NiCu slab. For reaction AB → A + B, the positive value suggests endothermic, while the negative value suggests exothermic.

Transition states (TS) are located by using the complete LST/QST method [31]. Firstly, the linear synchronous transit (LST) maximization was performed followed by an energy minimization in directions conjugate to the reaction pathway. The TS approximation obtained in that way is used to perform quadratic synchronous transit (QST) maximization. From that point, another conjugate gradient minimization is performed. The cycle is repeated until a stationary point is located. The convergence criterion for transition

Table 1
Vertical atomic displacements ($^{\Delta}z$, Å) for various surfaces of NiCu alloy.

	$^{\Delta}z(Ni^1)$[a]	$^{\Delta}z(Ni^2)$	$^{\Delta}z(Cu^1)$	$^{\Delta}z(Cu^2)$
Model A	0.048	0.011	−0.029	0.024
Model B	0.071	0.016	−0.013	0.016

[a] Ni^1 (Cu^1) and Ni^2 (Cu^2) denote Ni (Cu) atoms of the first and second layers, respcetively. $^{\Delta}z$ refers to the atomic displacement perpendicular to the surface. Negative $^{\Delta}z$ denotes an outward displacement, toward the vacuum; positive $^{\Delta}z$ denotes an atom movement in the direction of the bulk.

state calculations was set to: root-mean-square forces on atoms tolerance of 0.25 eV/Å.

3. Results and discussion

3.1. Surface properties

The calculated structural parameters of two model surfaces of the alloyed NiCu are collected in Table 1. On Model A and Model B, Ni atoms of the first layer (Ni^1) move inward (into the bulk) while Cu^1 atoms relax outward (to the surface) with respect to the computed bulk-terminated geometry. The vertical displacement $^{\Delta}z$ is larger for Ni^1 than for Cu^1 atoms: the values for Model A are 0.048 and 0.029 Å, respectively; the corresponding values of Model B are 0.071 and 0.013 Å. However, Ni and Cu atoms of the second layer (Ni^2 and Cu^2) both slightly move inward. From above results, we think that a little difference of geometry paramenters between Model A and Model B.

3.2. CH_4 dissociation

Nowadays, experimental researchers have proved the mechanism of CH_4 dissociation, i.e., sequential dehydrogenation, by detecting chemisorbed CH_3, CH_2 and CH on Ni (1 1 1) using secondary ion mass spectroscopy (SIMS) and X-ray photoelectron spectroscopy (XPS) techniques [32]. Theoretical calculations about CH_4 dissociation on metal surface, which are mainly focused on clean metal catalyst [33–37], also support the successive dehydrogenation mechanism.

On the other hand, theoretical studies have been paid much attention to CH_4 dissociation on Ni(1 1 1), collected in literature [38,39], which points out that there is discrepancy between the dissociation barriers of the first step for CH_4 dissociation for existent results obtained from periodic slab models. For example, Kratzer et al. [40] obtained that a dissociation barrier of about 1.04 eV (including zero point corrections), however, spin polar and the lattice relaxation are not considered. Jackson and co-workers [41] got that the dissociation barrier is 1.08 eV. Zhu et al. [42] reported that the activation energy is 0.91 eV, and it is lowered to 0.79 eV with the zero-point energy correction. We obtained that the dissociation barrier is 1.18 eV without zero point correction, which is consistent with Wang and co-workers [34]. The differences of barriers may ascribe to the models and methods employed.

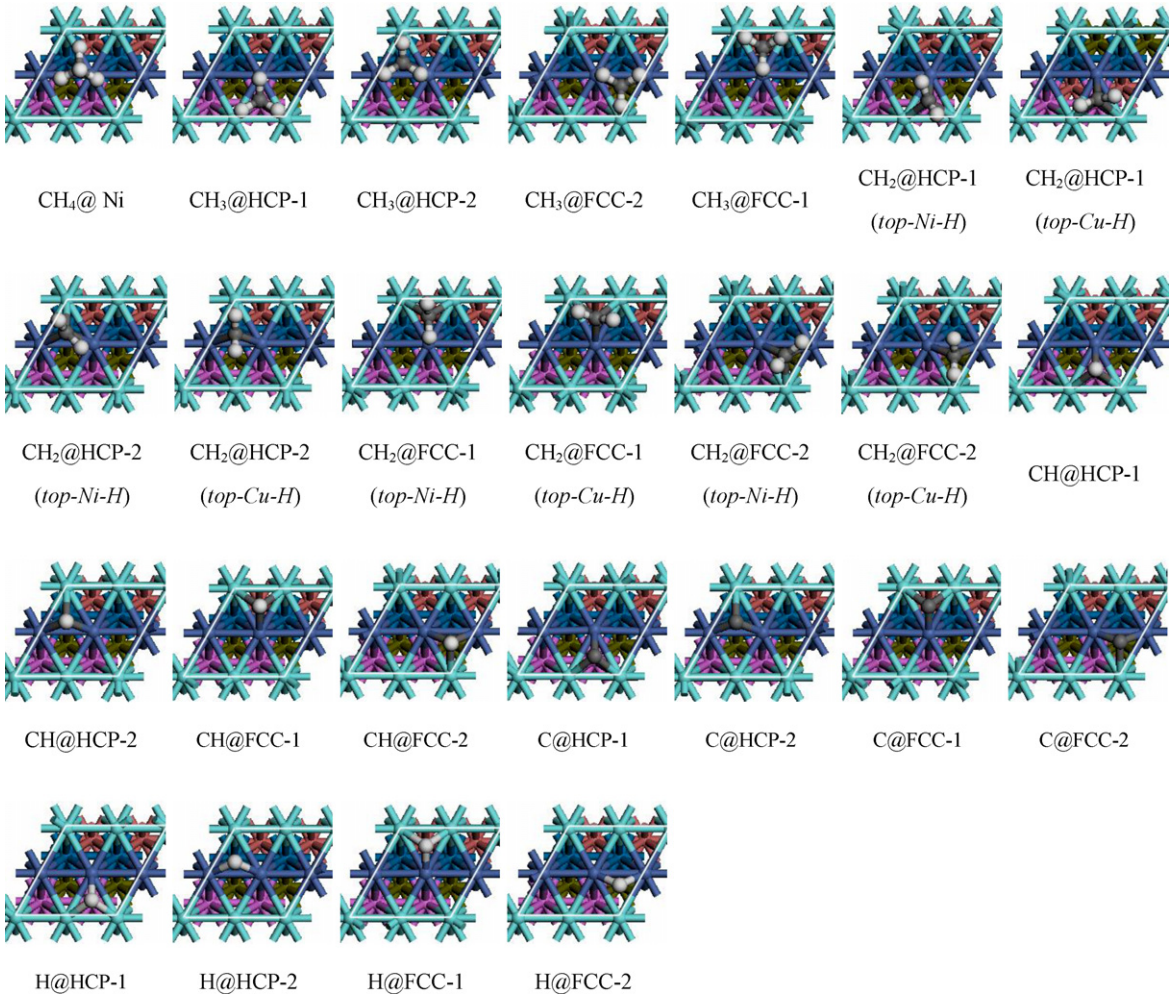

Fig. 2. The adsorption configurations of the CH_x(x = 0–4) on Model A of NiCu (1 1 1).

Table 2
Calculated adsorption energies (eV) of the CH*x* on the alloyed NiCu (1 1 1), Ni(1 1 1) and Cu (1 1 1) surfaces. (The energies in bold are the adsorption energies at the most stable adsorption sites).

	Ni(1 1 1)		Cu(1 1 1)		NiCu(1 1 1)									
	HCP	FCC	HCP	FCC	Model A				Model B					
					HCP-1	HCP-2	FCC-1	FCC-2	HCP-1	HCP-3	HCP-4	FCC-1	FCC-3	FCC-4
CH_3	−1.78	**−1.81**	−1.35	**−1.37**	−1.54	**−1.81**	−1.61	−1.77	−1.58	−1.60	−1.24	**−1.66**	−1.62	−1.39
CH_2	**−4.66**	**−4.66**	−3.85	**−3.91**	−4.20[a]	**−4.71**	−4.25	−4.70	−4.22	−4.27	−3.78	**−4.35**	−4.34	−3.93
					−4.30[a]	−4.67	−4.25	−4.66	−4.24	−4.27		−4.33	−4.27	
CH	**−6.24**	−6.15	−5.01	**−5.09**	−5.51	−6.18	−5.52	**−6.20**	−5.54	−5.58	−4.90	**−5.61**	−5.60	−4.99
C	**−6.90**	−6.80	−5.31	**−5.38**	−5.19	**−6.80**	−5.90	−6.74	−5.96	**−6.03**	−5.09	−5.98	−5.99	−5.08
H	−2.74	**−2.77**	−2.49	**−2.51**	−2.65	**−2.84**	−2.70	−2.81	−2.61	−2.68	−2.40	**−2.72**	−2.70	−2.51

[a] The adsorption energies for CH_2 in top-Ni-H and top-Cu-H, respectively.

Although differences exist, it does not affect our aim to compare the dissociation of CH_4 dissociaton on different NiCu catalyst surfaces. In addition, we also examined the CH_4 dissociation on Cu (1 1 1).

3.2.1. CH_x(x = 0–4) adsorption

There are four high-symmetry sites on the (1 1 1) surface of pure Ni: top (T), bridge (B), hexagonal-close-packed (HCP) and face-centered-cubic (FCC) threefold hollow sites. On the NiCu (1 1 1) surface, some additional sites are found because of the replacement of 50% Ni atoms by Cu and the Cu segregation on the surface. These adsorption sites are presented in Fig. 1.

3.2.1.1. CH_4 adsorption. Previous calculation results have proved that the adsorption energy of CH_4 is substantially small on transition metal surface, which may be negligible [43–45]. Here only one kind of geometry of CH_4 adsorption is considered on NiCu (1 1 1) surface, that is, three H atoms point to the surface, another H points to the surface normal (shown in Figs. 2 and 3). The calculated adsorption energies both are −0.02 eV on the two models, which are approximately equal to that on pure Ni (1 1 1) [38,39]. The molecule is positioned 3.678 Å above the surface on Model A and 3.556 Å on Model B. Obviously, the addition of Cu has little impact for CH_4 adsorption on the two surfaces of NiCu (1 1 1).

3.2.1.2. CH_3 adsorption. For CH_3 adsorption on aforementioned sites, there are two possible configurations with different azimuthal orientations: C—H bond pointing toward the nearest-neighboring metal atom or toward the midway between two neighboring metal atoms. Our previous study shows that there are almost no differences in energies and geometry parameters between the two configurations [46]. Herein, we only considered the former. On the other hand, CH_x(x = 0–3) prefers to adsorb at the threefold sites according to previous investigation, so we only consider the configuration that CH_x(x = 0–3) adsorb at the threefold sites in the following sections.

The adsorption of CH_3 on thses two models is first examined, and the adsorption energies at the threefold-hollow sites are listed in Table 2, along with the adsorption energies of CH_3 on pure Ni (1 1 1). The adsorption configurations on the two models are shown in Figs. 2 and 3.

There are four stable configurations obtained for CH_3 adsorbed at the threefold-hollow sites on Model A, while there are six stable structures on Model B. On HCP-1, HCP-3, FCC-1 and FCC-3 sites, CH_3 interacts with two Cu atoms and one Ni atom, while CH_3 is bonded to three Cu atoms on HCP-4 and FCC-4 sites, respectively. As shown in Table 2, it is clear that the order for adsorption energies of CH_3 on Model A is as follows: HCP-2 > FCC-2 > FCC-1 > HCP-1. However, the order on Model B is as follows: FCC-1 > FCC-3 > HCP-3 > HCP-1 > FCC-4 > HCP-4. On the other hand, for the most stable adsorption, it can be seen that Model A is energetically more favorable than Model B to adsorb CH_3, which in turn is more favorable than Cu (1 1 1). In addition, CH_3 has the approximately same adsorption energy on Model A as those on Ni (1 1 1) surface.

3.2.1.3. CH_2 adsorption. The calculated CH_2 adsorption energies at the threefole hollow sites are given in Table 2, and the adsorption configurations on the two models are shown in Figs. 2 and 3. The adsorbed CH_2 on HCP-1(3) and FCC-1(3) have two geometries, i.e., one H bonds to Ni (or Cu) atom, the other H atom points toward the midway of the metal–metal bridge (for clarity, they are denoted as top-Ni-H and top-Cu-H, respectively), which results in different activation characteristics of the two C—H bonds. For example, when CH_2 adsorbed on HCP-2 site, in top-Cu-H, the bond of C—H in which H pointing toward Cu atom is stretched to 1.114 Å, and another bond of C—H is only stretched to 1.109 Å, while the bond of C—H in which H pointing toward Ni atom is elongated to 1.114 Å and another bond of C—H is elongated to 1.103 Å in top-Ni-H. A similar configuration is also obtained on pure Ni (1 1 1) [34,47] and Cu (1 1 1) surface [48]. On NiCu (1 1 1), the most stable site for CH_2 adsorption on Model A is still HCP-2, while it is FCC-1 site on Model B. The adsorption energies become more negative from Cu (1 1 1) to Model B, and further to Ni (1 1 1) and Model A.

3.2.1.4. CH adsorption. CH is adsorbed at the threefold site with the remaining H atom oriented perpendicular to the NiCu (1 1 1) surface. It is noted that C moves to the nearby bridge site of Ni-Ni after geometry optimization on Model A, as shown in Fig. 2. From Table 2, we can obtain that addition of Cu decreases the adsorption energy of CH. CH adsorbed on Model A is more favorable than on Model B. The stability order for all configurations on Model A is as follows: FCC-2 ≈ HCP-2 > FCC-1 ≈ HCP-1, while that on Model B is FCC-1 ≈ FCC-3 ≈ HCP-3 > HCP-1 > FCC-4 > HCP-4.

3.2.1.5. C adsorption. Like CH adsorption, C also moves to the nearby bridge site of Ni-Ni after geometry optimization on Model A. On NiCu (1 1 1), the most stable site for C adsorption on Model A still is HCP-2, while it is HCP-3 site on Model B. The adsorption energies become more negative from Cu (1 1 1) to Model B, and further to Ni (1 1 1) and Model A. It is noted that the adsorption energy of the most stable adsorbed C is −6.03 eV on Model B, it is less negative by 0.77 eV than that on Model A, and by 0.87 eV than that on Ni (1 1 1). The decrease of C adsorption energy weakens the interaction between the carbon atoms and the surface, thus the formation of CO becomes more likely to prevent the building up of a graphite layer [49]. Therefore, we can conclude that Model B of NiCu (1 1 1) may suppress carbon formation.

3.2.1.6. H adsorption. Similar to CH and C adsorption on Model A, H also moves to the nearby bridge site of Ni-Ni after geometry optimization. However, the adsorption energy is more negative on Model A than that on Ni (1 1 1) and Model B, and it has the weakest adsorption on Cu (1 1 1).

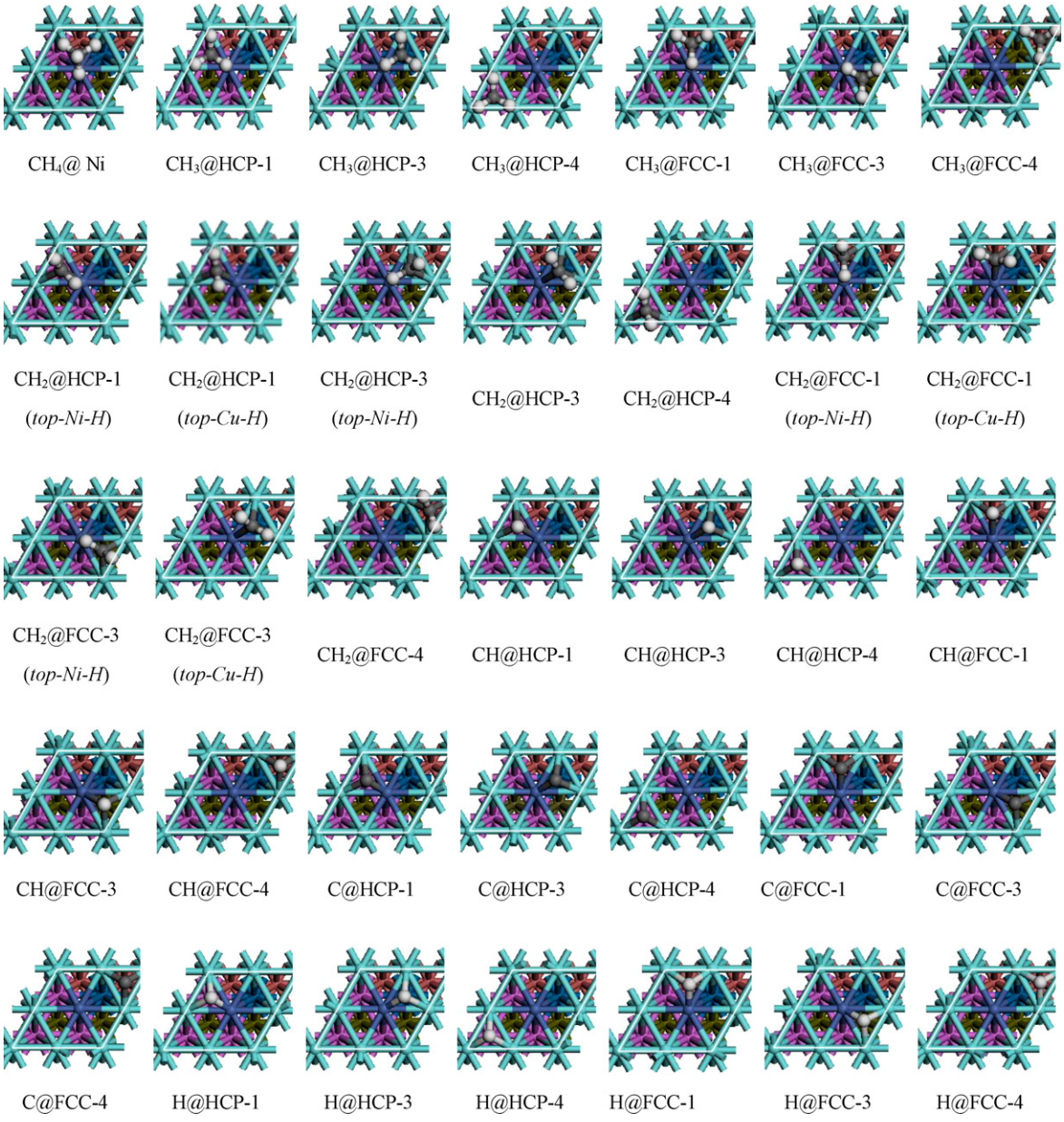

Fig. 3. The adsorption configurations of the CH_x(x = 0–4) on Model B of NiCu (1 1 1).

3.2.2. Mechanism for CH_4 dissociation

Cu is of very low reactivity respect to CH_4 dissociation compared to Ni. Therefore, Cu atom is not the active site. Herein, we only investigate the dissociation of CH_4 above Ni active site. CH_x(x = 1–4) can dissociate on the top of Ni into coadsorbed CH_{x-1} and H through different paths. The big difference between the paths is the coadsorbed Patterns of the products. These coadsorbed Patterns are shown in Fig. 4. On Model A, there are three coadsorbed Patterns for CH_{x-1} at HCP-2 and H at three three-fold sites separately. Pattern A1 and A3 are the coadsorbed CH_{x-1} at the HCP-2 site and H separately at the FCC-1 and HCP-2 site share one Ni in a zigzag way, while Pattern A2 is both the coadsorbed CH_{x-1} and H at FCC-3 sites share one Ni in a linear way.

On Model B, however, there are only two coadsorbed Patterns for CH_{x-1} at FCC-1 site and H at two different three-fold sites separately. Pattern B1 is that both CH_{x-1} and H adsorb at the FCC-1 sites and they share one Ni atom in a linear way. Pattern B2 is that CH_{x-1} adsorbs at the FCC-1 site while H adsorbs at the FCC-3 site, and they share a Ni atom in a zigzag way. The calculated coadsorption energies of CH_3 and H are listed in Table 3.

3.2.2.1. $CH_4 \rightarrow CH_3 + H$. From Table 3, we can clearly see that Pattern A3 is the preferred combination of CH_3 and H on Model A. The value of E_{ads} of the coadsorbed CH_3 and H (−4.45 eV) is slight lower than the sum of the values of E_{ads} for the isolated CH_3 and H (−4.65 eV), indicating the weak repulsive interaction between CH_3

Table 3
Co-adsorption energies (eV) at different patterns on the NiCu (1 1 1) surface.

	Model A			Model B	
	Pattern 1	Pattern 2	Pattern 3	Pattern 1	Pattern 2
CH_3 and H	−4.16	−4.43	−4.45	−4.12	−4.13
CH_2 and H	−7.05	−7.51	−7.44	−6.82	−6.85
CH and H	−8.53	−8.87	−8.85	−8.08	−8.13
C and H	−9.03	−9.38	−9.31	−8.28	−8.34

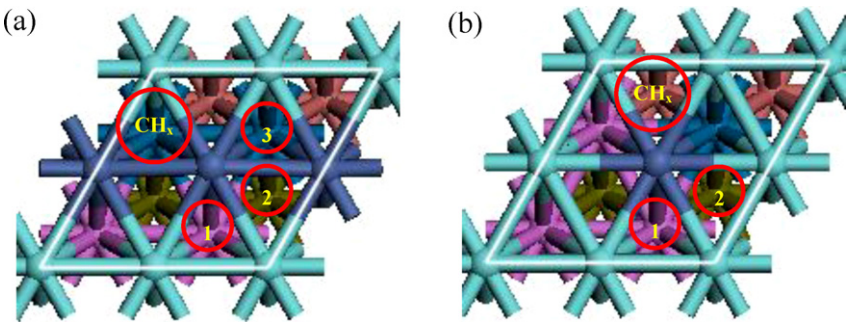

Fig. 4. The coadsorption Patterns of CH_x and H on NiCu (1 1 1). (a) Model A, (b) Model B.

and H. Thus, coadsorbed CH_3 and H in Pattern A3 are selected as the final state (FS) in CH_4 dehydrogenation. On Model B, Pattern B1 and B2 have the approximate coadsorption energies. Whearas, there exists a weaker repulsive interaction in Pattern B2 than that in Pattern B1. Therefore, the coadsorbed configuration of CH_3 and H in Pattern B2 is selected as the FS.

We take CH_4 physisorbed on NiCu (1 1 1) as initial state (IS) for studying CH_4 dissociatioin. On Model A, CH_4 can dissociation on the top of Ni into coadsorbed CH_3 and H through the transition state of TS A1 (shown in Fig. 5). In the TS A1, the CH_3 fragment and H both are bound at the top of Ni tilting to their own final threefold sites, the distances of C-Ni and H-Ni are 2.066 and 1.505 Å, respectively. This geometry resembles those of the activated complexes for CH_4 dissociation on Ni (1 1 1) and other close-packed transition metal surfaces [50,46]. This reaction is endothermic by 0.07 eV. The activation barrier is 1.09 eV, which is lower than those on pure Ni (1 1 1) [47] and Cu (1 1 1) [48].

On Model B, CH_4 also can dissociation on the top of Ni into CH_3 and H via the transition state of TS B1 (shown in Fig. 5), whose geometry resembles that on Model A. In TS B1, the distances of C-Ni and H-Ni are 2.205 and 1.474 Å, respecitvely. This reaction is an endothermic process with activation barrier of 1.32 eV, which is

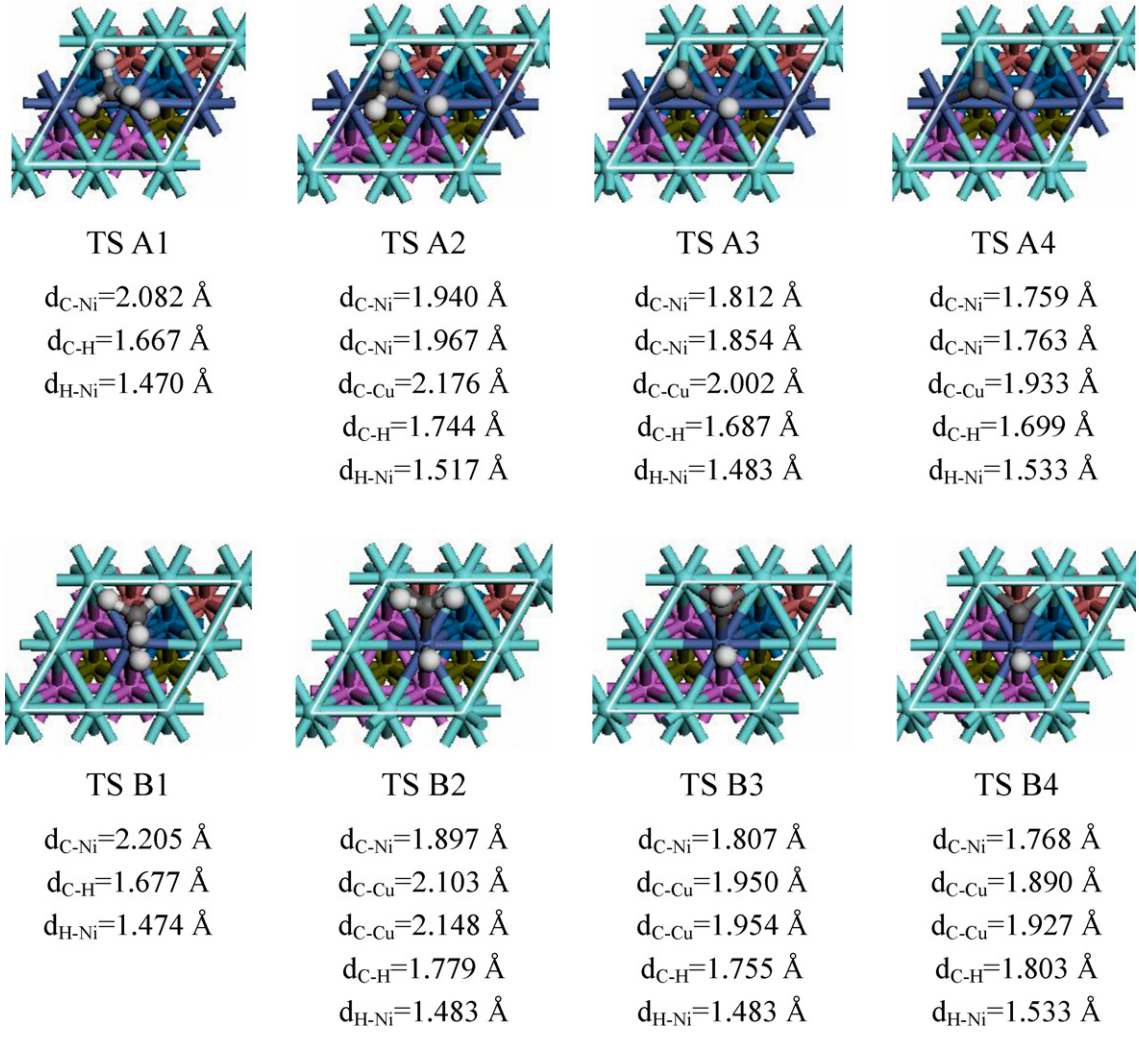

Fig. 5. The geometries and parameters of the transition states on the Model A and B of NiCu (1 1 1).

larger than our result on pure Ni (1 1 1) surface (1.18 eV) [47], but smaller than that on pure Cu (1 1 1) surface (1.88 eV). Obviously, the incorporation of Cu atoms into the Ni (1 1 1) affects the dissociation of CH_4, furthermore, the different morphology affects the reaction barrier.

3.2.2.2. $CH_3 \rightarrow CH_2 + H$. For co-adsorbed CH_2 and H, the lowest values of E_{ads} both are in Pattern A2 and B2 on Model A and B, respecitvely. As for the second dehydrogenation step, the TS configurations are similar to those on Ni (1 1 1) and other transition metal surfaces [50,46], in which the CH_2 fragments are located at their favorable adsorption sites and the detached H atoms are positioned at the adjacent threefold site. On Model A, the preferred reaction is endothermic by 0.05 eV and needs to overcome a low energy barrier of 0.66 eV, which is lower than that (0.77 eV) on pure Ni (1 1 1) [47] and that (1.47 eV) on Cu (1 1 1). In transition state TS A2, the distance between H and CH_2 are elongated to 1.744 Å from 1.121 Å in CH_3, and the forming bond of Ni-H is shortened to 1.517 Å. However, the reaction energy and the energy barrier on Model B are 0.32 and 0.77 eV, respectively. In transition state TS B2, the distance between H and CH_2 is increased to 1.779 Å from 1.121 Å in CH_3, and the forming bond of Ni-H is decreased to 1.483 Å.

3.2.2.3. $CH_2 \rightarrow CH + H$. Similar to the second step, the co-adsorbed CH and H in Pattern A2 and B2 are considered as the final states because of their higher coadsorption energies. In the third dehydrogenation step, CH_2 with top-Ni-H structure dissociates into CH and H. The reaction was exothermic by 0.36 eV with an activation barrier of 0.37 eV on Model A while it is thermal neutral with the energy barrier of 0.46 eV on Model B. In addition, the reaction barrier is 0.37 eV on Ni (1 1 1) [47] and 1.05 eV on Cu (1 1 1). In TS A3(B3), the separation between the cleaved H and the C atom is 1.687(1.755) Å, and the bond length of the H and Ni is 1.483(1.483) Å.

3.2.2.4. $CH \rightarrow C + H$. Similarly, the co-adsorbed C and H in Pattern A2 and B1 are considered as the final states in CH dehydrogenation step. The formation of surface C is accomplished by the dissociation of CH on the top of the surface Ni atom. The most preferred TS configurations (TS A4 and TS B4) on the two model surfaces are shown in Fig. 5. Both the two reactions are endothermic by 0.51 and 0.89 eV, and the activation barriers are calculated to be 1.37 and 1.63 eV on Model A and B, respectively. The former is approximately equal to that on Ni (1 1 1) while the latter is much higher than that on Ni (1 1 1). However, the activation barrier is 2.21 eV on Cu (1 1 1), higher than those on NiCu (1 1 1).

3.2.3. Enegetics of dissociation CH_4

For the purpose of elucidating the effect of the different active component surfaces on the kinetics of CH_4 dissociation and carbon deposition, the potential energy diagrams for CH_4 dissociation on the alloyed NiCu surfaces are compared with those on pure Ni (1 1 1) and Cu (1 1 1). According to reaction barriers (E_a) and reaction energies (ΔE) of successive dehydrogenation of CH_4, we plot the optimal potential energy surface, as displayed in Fig. 6. The sum of the total energies of the active component slab and free CH_4 molecules was taken as the origin.

From Fig. 6, we can see that, on Model A, the highest barrier for CH dissociation is 1.37 eV, while that is 1.63 eV on Model B. Obviously, the fourth step of CH_4 dissociation into CH_3 and H is the rate-determining step in CH_4 dissociation on Model A and B as well as on Ni (1 1 1) and Cu (1 1 1) surfaces. As a further comparison, the activation barrier of the rate-determining step on Model A is approximately equal to that on Ni (1 1 1), while the activation barrier is higher by 0.27 eV on Model B than that on Ni (1 1 1), but lower by 0.58 eV than that on Cu (1 1 1). It is well know that C is

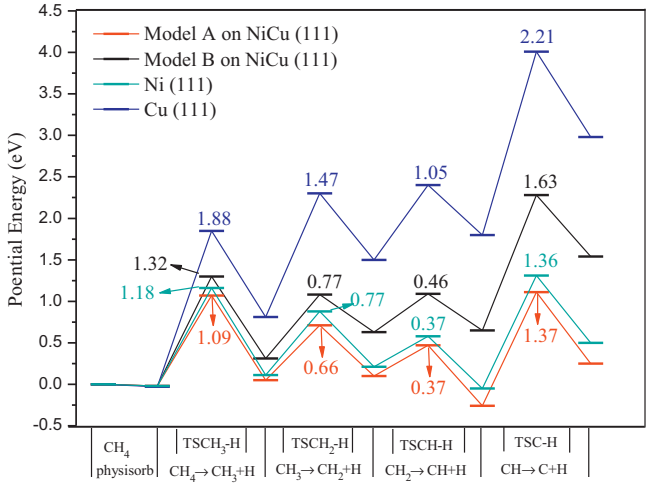

Fig. 6. Potential energy profiles of the CH_4 dissociation on different catalyst surfaces.

esay to form on pure Ni (1 1 1) at high temperature while it is difficult to form on Cu (1 1 1). Therefore, we think that C is favorable to form on uniform NiCu surface. However, it is unfavorable on Cu-rich NiCu surface. That is to say, Cu-rich NiCu surface can suppress the carbon deposition. Whereas, the uniform NiCu surface cannot suppress carbon deposition. Our results well explain the experimental facts described in Section 1.

4. Conclusions

In this work, we have conducted a DFT-based computational study on the dissociation of CH_4 on NiCu (1 1 1) bimetallic alloy models, and compare the results with those on pure Ni (1 1 1) and Cu (1 1 1). Two models, uniform surface (Model A) and Cu-rich surface (Model B), have been considered to express the NiCu (1 1 1) surface. The corresponding results on the two models have been compared with those obtained on pure Ni (1 1 1) and Cu (1 1 1) surfaces. On Model A, CH_x(x = 0–3) prefer to adsorb at the threefold sites to bond to two Ni atoms and one Cu atom while they prefer to adsorb at the threefold sites composed of one Ni and two Cu atoms on Model B. Moreover, the adsorption of C becomes stronger from Cu (1 1 1) to Model B, and further to Ni (1 1 1) and Model A, indicating that Model B can suppress carbon formation.

The rate-determining steps both are CH dissociation on the two models on the NiCu (1 1 1) surface. The activation barrier of the rate-determing step is 1.37 eV on Model A, approximately equal to that on Ni (1 1 1), while it is 1.63 eV on Model B, higher by 0.27 eV than that on Ni (1 1 1), but lower by 0.58 eV than that on Cu (1 1 1). Those indicate that C is easy to form on uniform NiCu surface. Conversely, it is unfavorable to form on Cu-rich NiCu surface.

Acknowledgments

The work was supported by the National Natural Science Foundation of China (grant no. 20976115) and the National Younger Natural Science Foundation of China (grant no. 20906066, 21103120).

References

[1] T. Osaki, T. Mori, Journal of Catalysis 204 (2001) 89.
[2] J. Xu, M. Saeys, Journal of Catalysis 242 (2006) 217.
[3] S. Tang, L. Ji, J. Lin, H.C. Zeng, K.L. Tan, K. Li, Journal of Catalysis 194 (2000) 424.
[4] D. Cheng, X. Zhu, Y. Ben, F. He, L. Cui, C. Liu, Catalysis Today 115 (2006) 205.
[5] J.H. Kim, D.J. Suh, T.J. Park, K.L. Kim, Applied Catalysis A 197 (2000) 191.
[6] E. Nikolla, J. Schwank, S. Linic, Journal of Catalysis 250 (2007) 85.
[7] J.H. Lee, E.G. Lee, O.S. Joo, K.D. Jung, Applied Catalysis A 269 (2004) 1.

[8] K. Takanabe, K. Nagaoka, K. Nariai, K. Aika, Journal of Catalysis 232 (2005) 268.
[9] D. San-José-Alonso, J. Juan-Juan, M.J. Illán-Gómez, M.C. Román-Martínez, Applied Catalysis A 371 (2009) 54.
[10] H.-W. Chen, C.-Y. Wang, C.-H. Yu, L.-T. Tseng, P.-H. Liao, Catalysis Today 97 (2004) 173.
[11] J. Zhang, H. Wang, A.K. Dalai, Journal of Catalysis 249 (2007) 300.
[12] H. Kim, C. Lu, W.L. Worrell, J.M. Vohs, R.J. Gorte, Journal of the Electrochemical Society 149 (2002) A247.
[13] S.-I. Lee, J.M. Vohs, R.J. Gorte, Journal of the Electrochemical Society 151 (2004) A1319.
[14] A. Christensen, A.V. Ruban, P. Stoltze, K.W. Jaclbsen, H.L. Skriver, J.K. Nørskov, F. Besenbacher, Physical Review B 56 (1997) 5822.
[15] A.R. Naghash, T.H. Etsell, S. Xu, Chemistry of Materials 18 (2006) 2480.
[16] S.M. Foiles, Physical Review B 32 (1985) 7685.
[17] S.C. Tsang, J.B. Claridge, M.L.H. Green, Catalysis Today 23 (1995) 3.
[18] J. Wei, E. Iglesia, Journal of Catalysis 224 (2004) 370.
[19] R. Zhang, B. Wang, H. Liu, L. Ling, Journal of Physical Chemistry C 115 (2011) 19811.
[20] F. Wang, D. Zhang, Y. Ding, Journal of Physical Chemistry C 114 (2010) 14076.
[21] S. González, C. Sousa, M. Fernández-García, V. Bertin, F. Illas, Journal of Physical Chemistry B 106 (2002) 7839.
[22] M.R. Notis, J. Brown, C.M. Cotell, C.E. Ells, G. Kalonji, M.H. LaBranche, V.C. Marcotte, T.B. Massalski, S.M. Merchant, J.E. Morral, C.A. Parker, A. Prince, G.D. Smith, M.S. Zedalis, Handbook of Alloy Phase Diagrams, 10th ed., ASM International, USA, 1996, pp. 745.
[23] V. Shah, T. Li, K.L. Baumert, H. Cheng, D.S. Sholl, Surface Science 527 (2003) 217.
[24] S.G. Wang, X.Y. Liao, J. Hu, D.B. Cao, Y.W. Li, J. Wang, H. Jiao, Surface Science 601 (2007) 1271.
[25] H. Liu, R. Zhang, F. Ding, R. Yan, B. Wang, K. Xie, Applied Surface Science 257 (2011) 9455.
[26] M.C. Payne, D.C. Allan, T.A. Arias, J.D. Joannopoulos, Reviews of Modern Physics 64 (1992) 1045.
[27] V. Milman, B. Winkler, J.A. White, C.J. Pickard, M.C. Payne, E.V. Akhmatsakaya, R.H. Nobes, International Journal of Quantum Chemistry 77 (2000) 895.
[28] J.P. Perdew, K. Burke, M. Ernzerhof, Physical Review Letters 77 (1996) 3865.
[29] D. Vanderbilt, Physical Review B 41 (1990) 7892.
[30] H.J. Monkhorst, J.D. Pack, Physical Review B 13 (1976) 5188.
[31] T.A. Halgren, W.N. Lipscomb, Chemical Physics Letters 49 (1977) 225.
[32] M.P. Kaminsky, N. Winograd, G.L. Geoffroy, M.A. Vannice, Journal of the American Chemical Society 108 (1986) 1315.
[33] J.E. Mueller, A.C.T. van Duin, W.A. Goddard, Journal of Physical Chemistry C 113 (2009) 20290.
[34] S.G. Wang, D.B. Cao, Y.W. Li, J. Wang, H. Jiao, Surface Science 600 (2006) 3226.
[35] N.M. Galea, D. Knapp, T. Ziegler, Journal of Catalysis 247 (2007) 20.
[36] M.S. Liao, Q.E. Zhang, Journal of Molecular Catalysis A 136 (1998) 185.
[37] M.F. Haroun, P.S. Moussounda, P. Légaré, Journal of Molecular Structure 903 (2009) 83.
[38] W. An, X.C. Zeng, C.H. Turner, Journal of Chemical Physics 131 (2009) 174702.
[39] C. Fan, X.-G. Zhou, D. Chen, H.-Y. Cheng, Y.-A. Zhu, Journal of Chemical Physics 134 (2011) 134704.
[40] P. Kratzer, B. Hammer, J.K. Nørskov, Journal of Chemical Physics 105 (1996) 5595.
[41] S. Nave, A.K. Tiwari, B. Jackson, Journal of Chemical Physics 132 (2010) 054705.
[42] Y.-A. Zhu, D. Chen, X.-G. Zhou, W.-K. Yuan, Catalysis Today 148 (2009) 260.
[43] Z. Zuo, W. Huang, P. Han, Z. Li, Applied Surface Science 256 (2010) 5929.
[44] J.M.H. Lo, T. Ziegler, Journal of Physical Chemistry C 112 (2008) 13642.
[45] D.C. Sorescu, Physical Review B 73 (2006) 155420.
[46] M.A. Vannice, Journal of Catalysis 50 (1977) 228.
[47] H. Liu, R. Zhang, R. Yan, B. Wang, K. Xie, Applied Surface Science 257 (2011) 8955.
[48] G. Gajewski, C.-W. Pao, Journal of Chemical Physics 135 (2011) 064707.
[49] F. Besenbacher, I. Chorkendorff, B.S. Clausen, B. Hammer, A.M. Molenbroek, J.K. Nørskov, I. Stensgaard, Science 279 (1998) 1913.
[50] T. Bligaard, J.K. Nørskov, S. Dahl, J. Matthiesen, C.H. Christensen, J. Sehested, Journal of Catalysis 224 (2004) 206.